Available online at www.sciencedirect.com
SCIENCE DIRECT®
European Journal of Pharmaceutics and Biopharmaceutics 57 (2004) 383–395
European Journal of Pharmaceutics and Biopharmaceutics
www.elsevier.com/locate/ejpb

Research paper

Determination of the physical state of norethindrone acetate containing transdermal drug delivery systems by isothermal microcalorimetry, X-ray diffraction, and optical microscopy

Silvia Latsch[a], Torsten Selzer[b], Lothar Fink[c], Jörg Kreuter[a,*]

[a]*Institut für Pharmazeutische Technologie, Johann Wolfgang Goethe-Universität, Frankfurt am Main, Germany*
[b]*Baxter Oncology GmbH, Frankfurt am Main, Germany*
[c]*Institut für Anorganische und Analytische Chemie, Johann Wolfgang Goethe-Universität, Frankfurt am Main, Germany*

Received 5 February 2003; accepted in revised form 8 September 2003

Abstract

Transdermal drug delivery systems (TDDS) enable a controlled drug delivery to the skin. The low permeability of the stratum corneum necessitates a high drug concentration of the polymeric matrix and often requires supersaturation. This, however, promotes crystallisation of supersaturated systems. Isothermal microcalorimetry at 25°C, polarisation light microscopy, and X-ray powder diffraction (XRPD) were used to characterise the crystal growth of norethindrone acetate (NEA). The solubility of NEA in the patches determined by these methods is about 4%.

The crystallisation process could be measured reliably and with a high accuracy by microcalorimetry and microscopy. XRPD was considerably less sensitive but was the only method allowing a semi-quantitative determination of the amounts of crystals formed. The drug-associated heat measured by microcalorimetry increased proportionally with increasing NEA concentration in the concentration range of 4–10% demonstrating a constant crystallisation rate. At a higher supersaturation, such as 12% drug content, the crystallisation process was accelerated. The application of Johnson-Mehl-Avrami kinetics for the analysis of nucleation and crystal growth of the punched patches indicated a site-saturated nucleation mechanism and a one-dimensional crystal growth. The crystallisation enthalpy of NEA was -22.8 ± 2.6 kJ/mol.

The most specific method to observe the crystal formation is polarisation light microscopy. However, the microscopic analysis requires much longer storage times than microcalorimetry to detect crystallisation.

Keywords: Norethindrone acetate; Transdermal drug delivery system; Crystallisation; Microcalorimetry; X-ray powder diffraction

1. Introduction

Only a limited number of drugs so far was employed for drug delivery using transdermal drug delivery systems (TDDS). These drugs are mostly dissolved in the adhesive matrix of the TDDS forming a solid solution but can also exist as a solid dispersion. One essential reason for the comparatively infrequent application of transdermal delivery is the barrier property of the skin, especially of the stratum corneum. Consequently, the bioavailability of topically administered drugs is very low. Hence, the required systemic doses normally should not exceed 20 mg/day [1].

Since it is difficult to achieve a sufficiently high flux rate across the skin, various methods of penetration enhancement are used. Besides chemical enhancement [1–2], which alters the barrier properties, or iontophoresis and phonophoresis (physical enhancement), the supersaturation of drugs in the patches is commonly employed to increase drug delivery, since diffusion across the skin is a passive process and the concentration gradient of the dissolved drug between the patch and the blood is the main driving force for the permeation: According to Fick's first law the permeation across the skin is proportional to the dissolved drug concentration in the patches, i.e. it directly depends on

* Corresponding author. Institut für Pharmazeutische Technologie, Johann Wolfgang Goethe-Universität, Marie-Curie-Straße 9, 60439 Frankfurt am Main, Germany. Tel.: +49-69-798-29682; fax: +49-69-798-29694.
E-mail address: kreuter@em.uni-frankfurt.de (J. Kreuter).

0939-6411/$ - see front matter © 2003 Elsevier B.V. All rights reserved.
doi:10.1016/S0939-6411(03)00158-9

the degree of supersaturation [2–7]. Another driving force for drug permeation is the affinity of the drug to the polymeric matrix and the tendency to leave the patch.

Supersaturation is defined as a state in which the dissolved amount of drug in the matrix exceeds its equilibrium solubility. Consequently, crystallisation occurs in patches with supersaturated drug concentrations in the polymeric adhesive shortly after storage [8–12]. The practical application of supersaturation as a tool for permeation enhancement in most cases is limited by this instability of the systems used. Since penetration of drugs through the skin only depends on their dissolved amount, the crystalline phase is inactive for permeation enhancement [11,13]. The thermodynamic activity of the resulting suspension having a saturated state is one; hence its flux through the skin is independent of the total concentration yielding a constant release [2,14].

In some cases crystallisation process can be largely prevented by the addition of polymers or different excipients; adversely it can be accelerated by crystallisation initiators. Ma et al. [15] for instance demonstrated that polyethylene glycol 900 (PEG 900) is a strong crystallisation initiator whereas polyvinylpyrrolidone (PVP) was found to be the most effective crystallisation inhibitor for norethindrone acetate.

The development of suitable transdermal patches as well as the investigation of their stability are time-consuming processes. Therefore, it would be very advantageous to find an easy analytical method enabling the fast and reliable measurement of crystallisation processes. This would significantly facilitate the determination of the long term stability and, therefore, may accelerate TDDS development.

Isothermal heat conduction microcalorimetry is a very sensitive technique enabling detection of small amounts of heat [16]. All physical, chemical, and biological processes, like crystallisation or decomposition processes which are the main reasons for the instability of TDDS, are accompanied by heat evolution or absorption. Therefore, a variety of crystallisation processes were already detected by microcalorimetry [17–33]. Because of the high crystallisation energies it is possible to measure the crystal growth in transdermal patches by this method even at 25°C, whereas for the determination of a number of other reactions accelerated conditions at higher temperatures have to be employed.

In previous studies microcalorimetry was already applied to analyse enthalpy of precipitation [19,20,24,28,30,33]. The total heat liberated during precipitation of 1 mol of a crystalline substance was obtained by integration of heat flow curves. Besides the determination of thermodynamic parameters microcalorimetry also enables to measure reaction kinetics such as crystal-growth rates [17,34] relative to the degree of supersaturation.

2. Theoretical development

Crystallisation generally consists of two different processes, namely nucleation and crystal growth. The isothermal crystallisation kinetics was originally described by the Johnson-Mehl-Avrami (JMA) equation [35–40]:

$$x(t) = Q(t)/Q_\infty = 1 - \exp(-kt^n) \quad (1)$$

in which $x(t)$ represents the crystallised fraction at time t corrected by the induction time, n is known as the Avrami exponent, and k is the rate constant of isothermal crystallisation with physical unit $[(\text{time})^{-n}]$ dependent on the exponent n. The Avrami exponent is a characteristic parameter of the nucleation and of the growth mechanisms of crystals as well as of the number of directions (dimensionality) in which growth occurs and with it favoured crystal shape (Table 1).

The values for k and n can graphically be determined by the classical double-logarithm expression of Eq. (1):

$$\ln[-\ln(1 - x(t))] = n \ln t + \ln k \quad (2)$$

The graphs of $\ln[-\ln(1 - x(t))]$ versus $\ln t$ should generate a straight line over a wide range of the transition from amorphous to crystalline provided that no change in the crystallisation mechanism occurs. The slope corresponds to the Avrami exponent n. Comparison of the rate constants using this formula is not an accurate approach due to the different dimensions applied, therefore, another more suitable formula was developed [34,41,42]:

$$x(t) = 1 - \exp\left[-(k^* t)^n\right] \quad (3)$$

Table 1
Values of the Avrami exponent n derived for different nucleation and growth mechanism (from refs. [34,38,43])

Nucleation growth rate	Continuous interface controlled	Continuous diffusion controlled	Site saturated interface controlled	Site saturated diffusion controlled
One dimension	2	3/2	1	1/2
Two dimension	3	2	2	1
Three dimension	4	5/2	3	3/2

The physical dimension of the crystallisation rate constant k^* is time^{-1}. The values of k and k^* are different but can be converted to the uniform unit time^{-1} valid for one dimension by using the following conversion formula.

$$k^{1/n} = k^* \quad (4)$$

3. Materials and methods

3.1. Materials

Norethindrone acetate (NEA), PEG 400, pressure sensitive acrylate adhesive dissolved in ethyl acetate (Durotak® 387–2287, National Starch & Chemical B.V., Zutphen, Netherlands), backing membrane (Hostaphan® RN 23), release liner (Hostaphan® RN 100) as well as the semi-permeable membrane Cotran® 9728 were obtained as a gift from Lohmann Therapiesysteme LTS (Andernach, Germany). The Hostaphan foils (Mitsubishi Polyester Film GmbH, Wiesbaden, Germany) consist of polyethylene-terephthalat whereby thickness in μm is given by the number. Hostaphan® RN 100 is siliconised on both sides for better removal. The semipermeable Cotran® 9728-membrane (3M Drug Delivery Systems, Borken, Germany) in contrast consists of poly(ethylene-co-vinylacetate) containing 19% vinylacetate and having a thickness of 50.8 μm.

The solvents ethyl acetate, methanol and tetrahydrofurane (THF) were provided by Merck Eurolab (Darmstadt, Germany). Deionised water was made by Ultra-pure Water System Milli-Q plus.

3.2. Preparation of TDDS

The TDDS were prepared as described before [12] using NEA instead of E2-hemihydrate and stored at room temperature.

To determine the saturation solubility of NEA in the acrylic matrix special two-layer-laminates which were separated by a semi-permeable Cotran® 9728 membrane were prepared. One layer contained the drug while the other one consisted of a drug free acrylic polymer patch. These laminates were also stored at room temperature so that the solved drug molecules could diffuse to the placebo side until saturation was achieved. Excessive drug crystallisation occurred on the drug side confirming supersaturation. After reaching the equilibrium of concentration the initially drug-free system was removed from the Cotran® 9728 membrane and the concentration of NEA was determined by HPLC.

3.3. Polarisation microscopy, microcalorimetry, and X-ray powder diffraction (XRPD)

Polarisation microscopy, microcalorimetry, and X-ray analysis were performed as described before [12].

3.4. HPLC analysis

HPLC analysis of NEA was performed using a Hitachi L-6220 intelligent pump, set at a flow rate of 0.8 ml/min, a LaChrom auto-sampler L-7200, a LaChrom column oven L-7350 maintained at 40°C, a LC-Spectrophotometer Lambda-Max 481 variable wavelength UV detector set at 245 nm and a KONTRON PC-integrator version 3.9. The stationary phase was a Hibar 250-4 C-18 reversed phase packed column. The mobile phase consisted of methanol: THF: water with the percentage of 15:22:63 in the beginning and was switched after 49 min to a ratio of 25:25:50.

Calibration was performed by threefold injection of a standard solution containing 1.0 mg/ml NEA. The calibration coefficient amounted to 1.1054 ± 0.0224 mV·min·ml/μg using an injection volume of 20 μl. The retention time of NEA was 40 min. The same method was used to detect possible decomposition products of NEA, i.e. nordion, 6β-hydroxy-NEA, 6α-hydroxy-NEA, and norethindrone, after storage at 25°C. The relative retention times compared to NEA were 0.30, 0.35, 0.43, and 0.49, respectively.

3.5. Differential scanning calorimetry

Differential scanning calorimetry (DSC) was performed using DSC-7 (Perkin Elmer, Germany) in the range 20–220°C. The runs were conducted with heating rates of 10, 20, 30, and 40°C/min. Measurements were made in an atmosphere of nitrogen of 1.4 bar. Temperature and area calibration was done by indium and zinc. Approximately 10 mg of sample were accurately weighed in aluminium pans. The measured values are given as onset values.

4. Results and discussion

4.1. Polarisation microscopy

The crystallisation of amorphous NEA in the patches was observed visually as well as by polarisation light microscopy at a drug concentration ranging from 4 to 12%. It was found that the laminates were amorphous and free from crystals directly after their manufacture. After a relatively short induction time of 5 weeks for the laminates containing 4% NEA and 1 day only for the 12% NEA patches crystallites were formed which could be observed by microscopy. For low concentrations a longer induction time was obvious while increasing contents resulted in a faster crystal nucleation and crystal growth as already described for estradiol hemihydrate [12]. Consequently, the crystal nets became denser due to these crystallisation

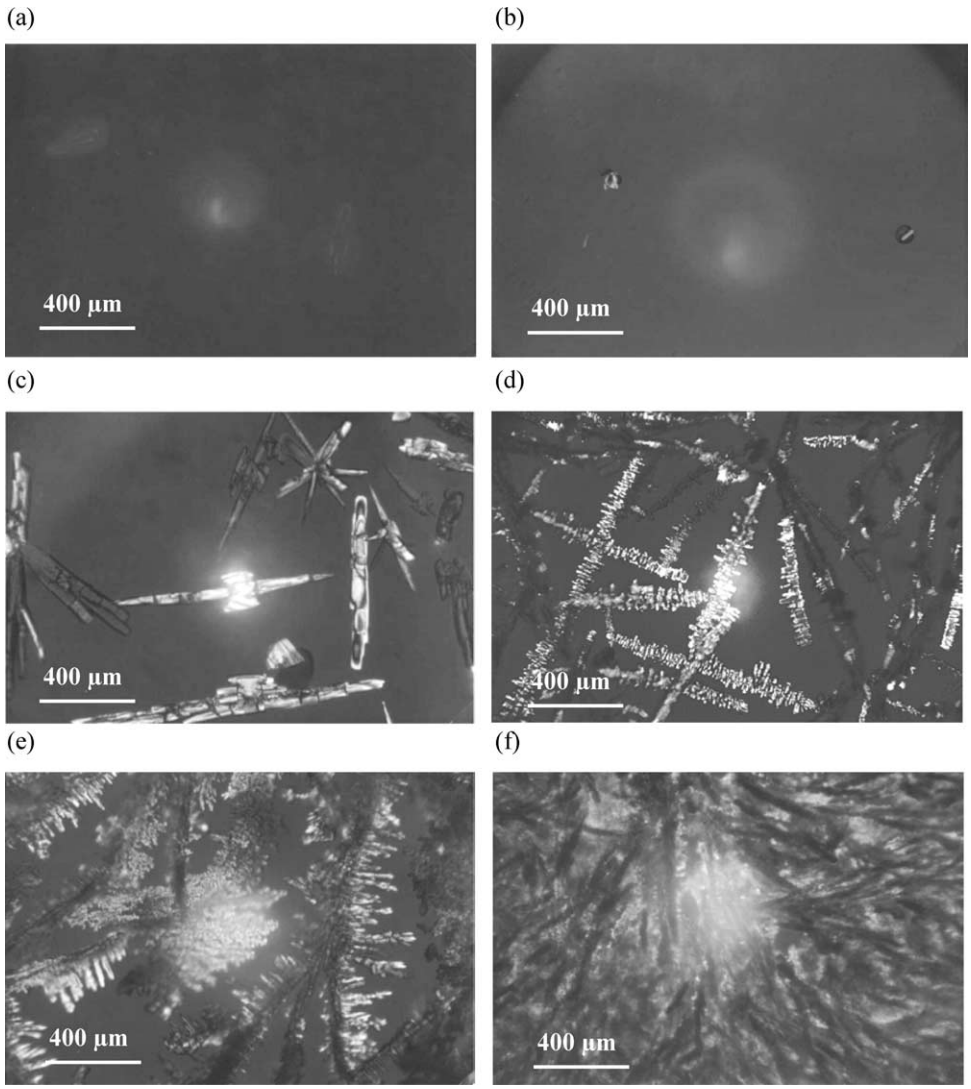

Fig. 1. Polarisation microscopy of NEA containing TDDS with increasing drug concentration, storage at room temperature: (a) 2%, 12 months; (b) 4%, 12 months; (c) 6%, 8 weeks; (d) 8%, 8 weeks; (e) 10%, 8 weeks; and (f) 12%, 1 week.

processes and the crystal quantity increased with the drug concentration at storage (Fig. 1).

The laminate containing NEA with a concentration of 2% did not generate any crystals in the matrix and remained amorphous during a storage period of 12 months (Fig. 1a) whereas in the 4% NEA patches only some small crystals were formed (Fig. 1b) within the same time period. Following these results it can be assumed that the saturation of NEA (C_{sat}) in the acrylic matrix will be obtained at a concentration only somewhat less than 4%.

It was found that NEA crystallises in a stick-like morphology. At high degrees of supersaturation the sticks develop a dendritic growth pattern in contrast to estradiol which crystallised in a needle-like structure [12].

4.2. X-ray powder diffraction (XRPD)

The crystallisation processes at a constant temperature were also examined by XRPD. Directly after preparation the transparent matrix did not show any characteristic peaks caused by a crystalline matrix (Fig. 2a). The only remarkable broad peak observed at 21.3° 2θ arose from the semi-crystalline sample holder's plastic support which of cause was not eliminated by the amorphous background subtraction. Due to the manual clamping of the plastic support into the sample holder the peak size will vary according to how tight the plastic support is stretched.

However, during the storage of one batch of a 10% NEA containing patch at room temperature increasing reflection patterns appeared due to the crystallisation of the drug whereas the polymeric patch matrix remained amorphous. The X-ray diffraction patterns of the crystals with typical peaks at 14.8° 2θ (triplet), 16.5° 2θ, and 20.8° 2θ correspond fully to the pattern of pure NEA (Fig. 2). As with estradiol hemihydrate in the previous studies [12] the crystal structure was not changed in the polymeric matrix.

XRPD was used to quantify the crystal growth in the amorphous matrix [12]. This quantitative analysis is based

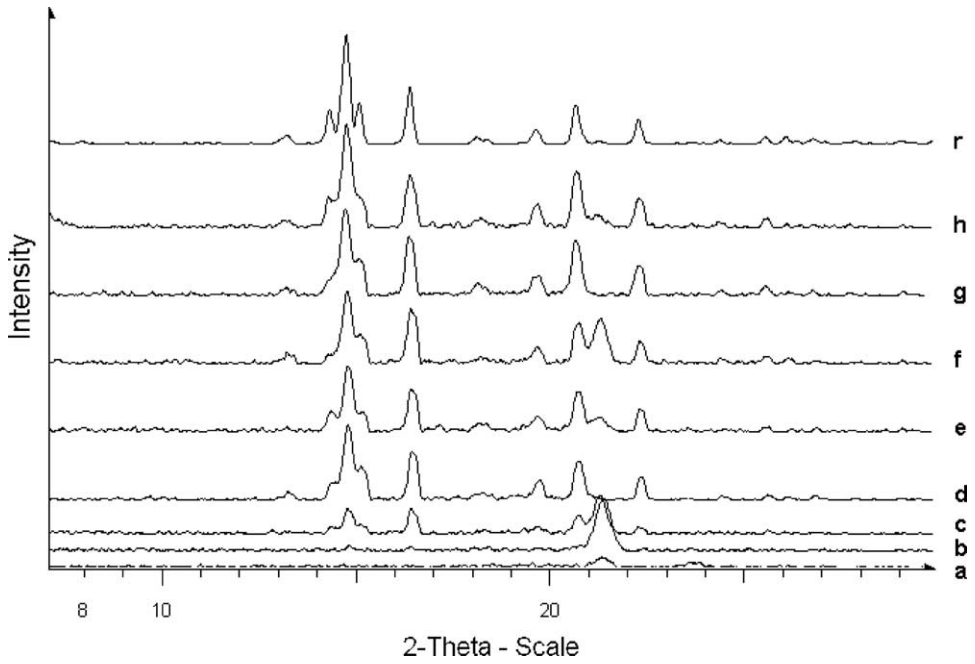

Fig. 2. X-ray diffraction pattern (with correction of the amorphous background) of 10% NEA containing TDDS, storage at room temperature: (a) 0 day; (b) 1 week; (c) 2 weeks; (d) 4 weeks; (e) 6 weeks; (f) 8 weeks; (g) 3 months; and (h) 4 months, (r) pure NEA as reference. The unsteady peak appearing at approximately 21.3° 2θ was caused by the sample holder's plastic support.

on the assumption that integrated net intensities of the reflections are directly proportional to crystal concentration (Fig. 3). The triplet at 14.8° 2θ shows the greatest net peak area, i.e. the highest sensitivity and, consequently, the lowest error can be expected at this reflection (Fig. 3a). Therefore, it was preferably used for the analysis. Because of the great width of the peaks obtained at the typical position of 20.8° 2θ this reflection sometimes is not separated from the peak of the sample holder at 21.3° 2θ. Despite of this a high logarithmic correlation exists in Fig. 3c.

The start of the drug crystallisation, i.e. nucleation and formation of small germs observed by microscopy, was not detectable by XRPD. The initially generated small crystals only have a small number of molecule planes reflecting the X-ray beam which causes low intensities and broad peaks. These very low peak intensities of small crystal germs disappear completely in the amorphous background noise. Therefore, no reflection areas were detectable by this method after 1 week of storage whereas by microscopy crystals were observed already after this time.

The reflection intensities increased continuously with storage time corresponding to the higher crystal amount generated within the matrix until the crystallisation process was completed after 3 months (Fig. 3). As expected it was found that the intensities of the XRPD reflections increased with drug concentration.

However, crystal growth was only reliably detectable by XRPD at concentrations of $\geq 8\%$ NEA in the matrix. In contrast, by microscopy crystal germs were already visible after 5 weeks at a drug concentration of 4% representing a considerably lower sensitivity of XRPD.

It was already mentioned that different samples of the same laminate cast gave considerably different peak intensities with XRPD because nucleation processes runs randomly, and the crystals are not homogeneously distributed over the patch area [12]. To largely eliminate errors, logarithmic regression lines were fitted to the X-ray reflection area vs. time curves of the measured XRPD-data for the typical reflections at 14.8°, 16.5°, and 20.8° 2θ to calculate the theoretical net peak area for the storage time point 13 weeks (Fig. 4). This plot shows a nearly linear correlation between the calculated net peak area and the NEA loading for the typical reflections at 14.8° and 16.5° 2θ. As shown in Fig. 4, the extrapolation of the linear regression lines to the x-axis lies between a total content of NEA 4.5 and 5.6% and indicates the saturation solubility. The determination of the saturation solubility by XRPD results in a relatively wide concentration range, possibly as a consequence of the comparable strong fluctuations of the measurements. Additionally a stronger crystal growth at higher supersaturations associated with stronger texture effects in the matrix also can result in deviations from linearity. The reflection at 16.5° 2θ shows a weaker linear dependence ($R^2 = 0.69$) but more a logarithmic one ($R^2 = 0.79$) associated with a higher intersection with x-axis at 5.4% NEA very close to the reflection at 14.8° 2θ. Hence, the saturation solubility of 5.5% determined by this method is 1.5% higher than by polarisation microscopy due to the lower sensitivity of XRPD for small crystal germs.

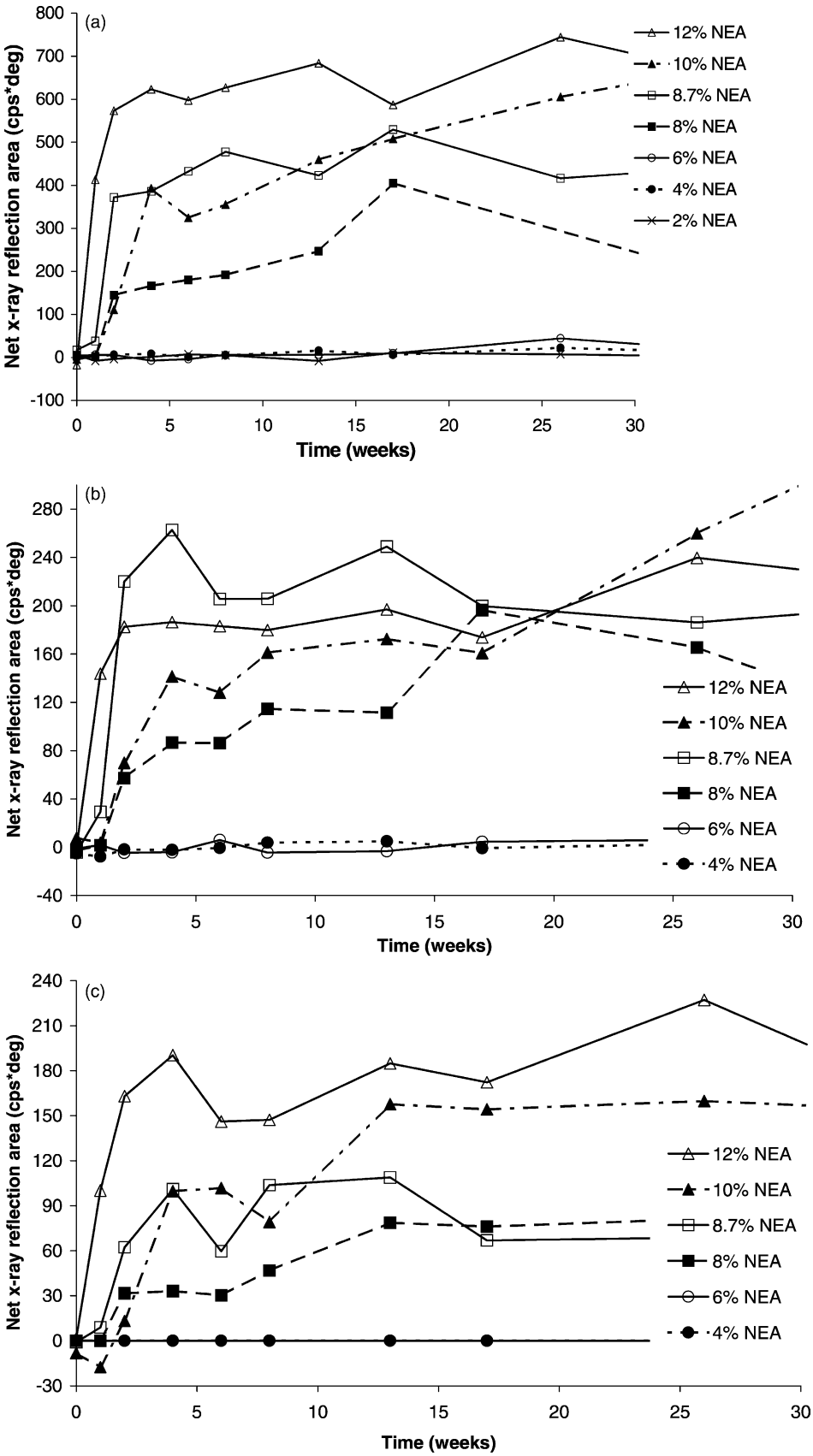

Fig. 3. X-ray reflection net area for the characteristic NEA peaks at (a) 14.8° 2θ; (b) 16.5° 2θ; and (c) 20.8° 2θ in dependence of the NEA content within the patch and the storage time at room temperature (standardisation on matrix area weight of 100 g/m^2, constant layer thickness).

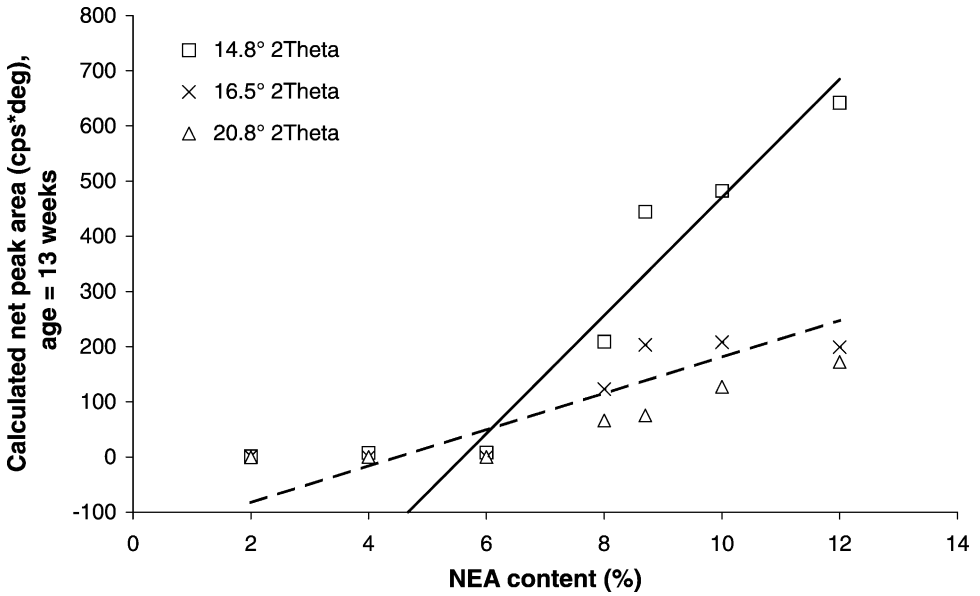

Fig. 4. Dependence of the calculated net peak area after 13 weeks of storage from the NEA content. Concentrations without measured crystallisation are not included in the linear regression.

4.3. Microcalorimetry

The crystallisation process also was examined by isothermal heat conduction microcalorimetry. As expected, the measurable drug-associated heat flow after subtraction of the placebo-induced heat flow increased with the drug concentration, confirming an increase in amount of crystals (Fig. 5).

While no crystal growth was observable at a NEA concentration of 2% by using microscopy, a low drug-associated heat flow of 0.15 μW/g matrix mass could be detected by microcalorimetry, i.e. a certain drug instability in the patches was indicated at this very low concentration. Although very sensitive, microcalorimetry is non-specific and does not provide any information on the cause for this instability. The main decomposition product of NEA is 6β-hydroxy-NEA. It increased by about 0.2%/year. However, since nearly no chemical decomposition was seen by HPLC and since no recrystallisation occurred within a period of 1-year, we assume that this small heat flow was an analytical error in the microcalorimetric measurements within the measurement inaccuracy.

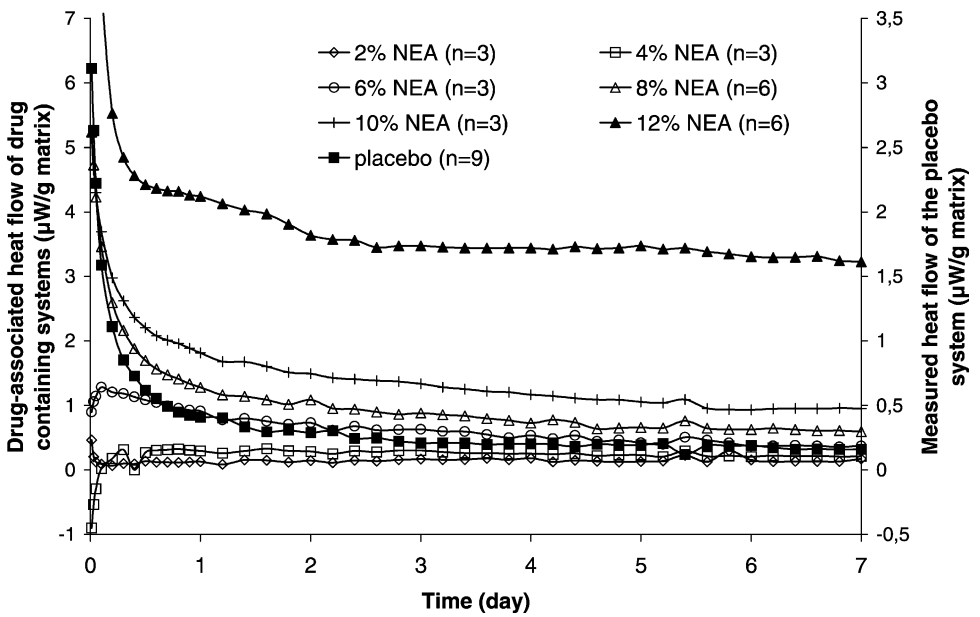

Fig. 5. Concentration dependent drug-associated heat flow of NEA containing TDDS and placebo heat flow (at 25°C).

It was found that patches with a drug concentration of 4% evolved a drug-associated heat flow of 0.2–0.3 μW/g matrix mass within a period of 1–7 days, while the crystallisation process was detectable by microscopy only after 5 weeks. This clearly demonstrates the great advantage of the microcalorimetric method for exploring crystallisation at very early stages. On the other hand, microscopy is more specific and enables a more detailed morphological analysis of the crystal formation.

In order to load the measuring ampoules with the patches, small discs of a diameter of 10 mm had to be punched out. Unfortunately, the shear force required for cutting these disks initiated a stronger crystallisation at the edges of the patches confirmed by microscopy and induced a high initial heat flow [8,12]. Subsequently, the crystal growth and consequently the drug-associated heat flow decrease continuously (Fig. 5). No second separate heat flow maximum was observed which would be an indicator for supplementary nucleus formation. Therefore, it can be assumed that only crystal growth but no significant formation of crystal germs occurred inside the punched laminate.

Assuming that the first 24 h of the microcalorimetric analysis were strongly affected by the cutting effects, the total crystallisation heat Q (J) and the initial drug-associated heat flow $dQ_{t=0}/dt$ (μW) were calculated by correlation functions of the heat flow versus time curve using the time interval between 1 and 7 days [12]. In agreement with the results of the microscopical investigations and X-ray diffraction microcalorimetry shows an increasing drug-associated heat evolution and initial heat flow with rising drug concentrations (Fig. 6).

In theory, a linear correlation should exist between drug content and evolved heat provided that the crystallisation process runs at the same rate [12]. Linearity of drug-associated heat and initial heat flow indeed was obtained over the measuring period of 7 days for patches containing a drug concentration of 4–10% NEA (Fig. 6). This seems to be an isokinetic concentration range above saturation solubility having the same rate of crystallisation. An isokinetic range of temperatures and concentrations exists for a given substance and crystal habit in which the characteristic kinetics of phase change remains constant [44]. It was found that at a higher drug content, i.e. 12% NEA, more heat was released than theoretically expected. The heat increased approximately by a factor of 2.6 whereas the NEA content only increased by a factor of 1.2, i.e. from 10 to 12% (Fig. 6). Therefore it has to be concluded that crystallisation process was accelerated at this very high degree of supersaturation because of the exceptional high thermodynamic instability (see below). The heat of the 2% NEA containing system does not lie in the linear range considering the linear regression line in Fig. 6.

The short measurement period of 7 days does not enable the determination of the crystallisation enthalpy ΔH_{cry} of NEA because the crystallisation process was not completed. Therefore, a test period of 4 weeks was necessary to cover the essential part of the crystallisation heat for the various patches examined (Fig. 7). This period was found to be sufficient to calculate a reliable and accurate enthalpy value. The slope of the linear curve results in a crystallisation enthalpy of NEA of -22.8 ± 2.6 kJ/mol in the acrylic matrix containing 7.1% PEG 400. Displayed data represent the average value of two runs.

The drug-associated heat flow decreases continuously during the crystallisation process. However, a constant low exothermic heat flow still was measurable even after 4 weeks in all examined patches independently of the initially

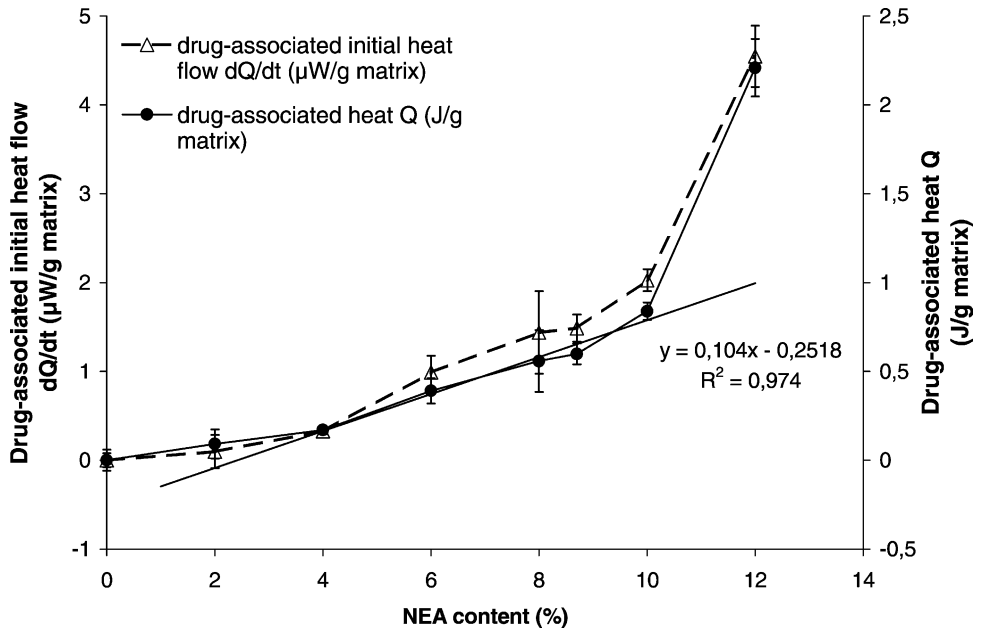

Fig. 6. Correlation between calculated 7 days drug-associated heat and the initial heat flow in dependence of NEA content (at 25°C).

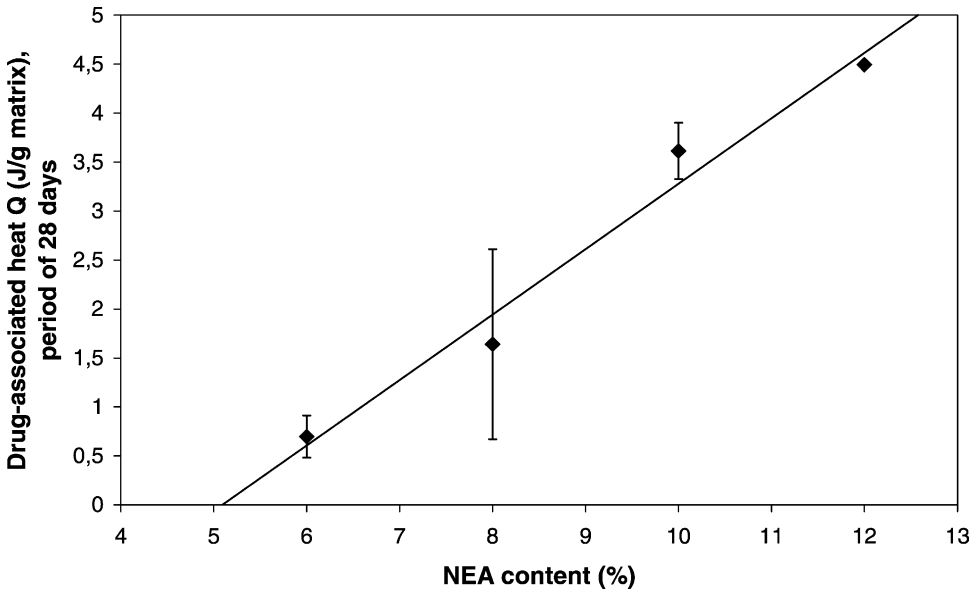

Fig. 7. Linear correlation between drug-associated heat in dependence of NEA content over a long measurement period of 28 days (at 25°C).

used drug concentration. Assuming that after this period the same heat quantities evolved, the difference between the measured crystallisation heat released from the samples with various drug concentration remains the same. Therefore, the examination was terminated after 4 weeks.

4.4. HPLC

The saturation concentration of NEA in the patches also was determined by HPLC after equilibration between a supersaturated patch containing NEA and an initially drug-free patch, mounted together but separated by a semi-permeable membrane. In using drug concentrations of 8 and 10% NEA, respectively, an average saturation solubility of 3.85% was measured (Table 2) which is in agreement with the microscopically determined solubility of $\leq$4%.

4.5. Crystallisation kinetics

Microcalorimetry also enables the determination of kinetic reaction parameters like reaction order and rate constants including crystallisation rate constants [34,45–49]. Crystallisation kinetics is described by the JMA equation [Eq. (1)]. In the following it shall be tried to apply the JMA-kinetics to the measured microcalorimetric data. Therefore, it was assumed that the heat production by crystallisation was proportional to the amount of recrystallised drug. To calculate the crystallised fraction $x(t)$ of NEA at time t from the evolved heat $Q(t)$, the saturated solubility C_{sat} and the crystallisation enthalpy ΔH_{cry} were used to obtain the theoretical total heat at the end of the crystallisation process Q_∞ [Eq. (1)]. Fig. 8 shows the crystallised fraction as a function of time t. At a constant crystallisation rate nearly the same crystallised fraction of 0.2 was formed after 1 week in the concentration range of 6–10% NEA. Patches with a drug concentration of 12% showed a higher crystalline fraction due to an accelerated crystallisation process.

In Fig. 9 the crystallised fraction was plotted against time using the linear expression of the JMA-equation [Eq. (2)]. The linear Avrami correlation [Eq. (2)] enables the calculation of the growth rate parameters k as well as n (Table 3).

The value of the Avrami exponent n is nearly constant, approximately 0.75. The low value of n confirms a one dimensional needle-like crystal growth and a site saturated nucleation (see Table 1). This would indicate that all nuclei are already present at the beginning of the isothermal measurements, and almost no additional nuclei are formed during the microcalorimetric measurement. This result is corroborated by the continuously decreasing heat flow curve. The tailing of the isothermal calorimetric curves can be related to a diffusion-controlled growth and the expected n value would be 0.5 [43]. However, the measured value of 0.75 indicates that still some nucleation is going on for some time.

The rate constant k^* was determined as 0.02 1/d in the average and did not change within the concentration range of 6–10% NEA. However, patches containing 12% drug

Table 2
Saturation concentration of NEA determined by HPLC (after a storage period of 2 month)

NEA content at time zero (%)	NEA content of the placebo layer after storage (%)
8	3.6
10	4.1

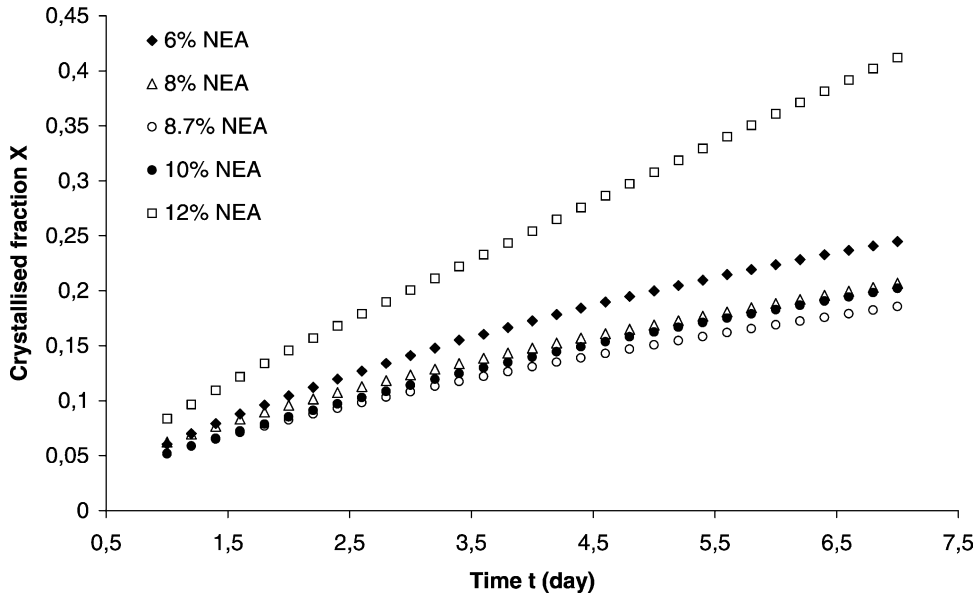

Fig. 8. Dependency of the calculated crystallised fraction of NEA containing TDDS with time.

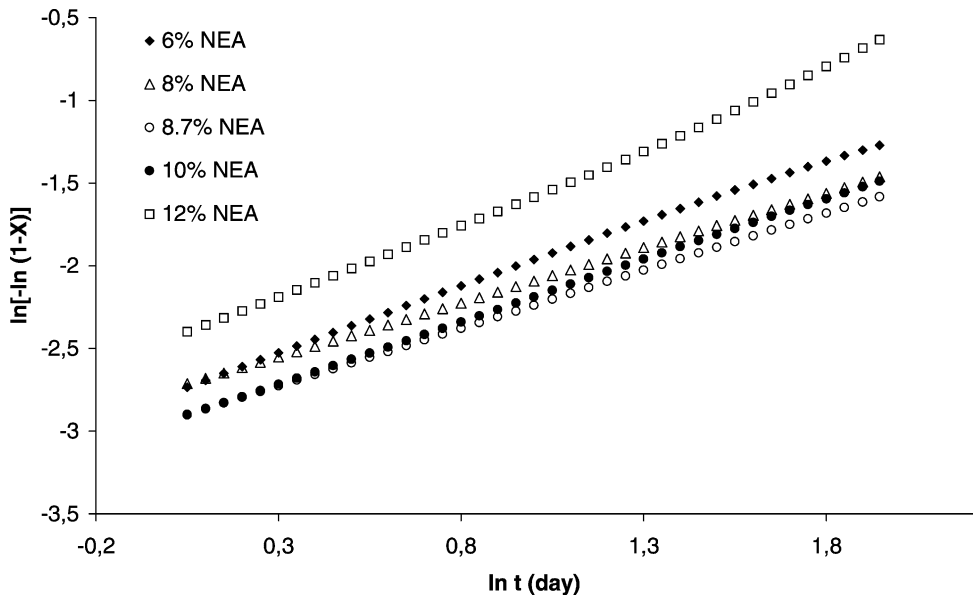

Fig. 9. NEA crystallisation data plotted using the classical double-logarithm Avrami plot for determination of exponent *n* and rate constant *k*.

showed an accelerated crystallisation process which could be associated with the higher rate constant of 0.07 1/d. This is in accordance with Ma et al. [15] who reported that the rate of crystallisation and the number of crystals increased with a rising drug content.

4.6. Differential scanning calorimetry (DSC)

DSC also should be able to differ between the amorphous or crystalline state of NEA within the patches and to quantitatively determine crystals using the peak area of

Table 3
Avrami parameters experimentally derived for NEA crystallisation (different concentrations in the acrylic matrix)

NEA content (%)	Avrami exponent *n*	*k* (1/d^n)	*k** (1/d)
6.0	0.7873	0.0628	0.0297
8.0	0.6574	0.0642	0.0153
8.7	0.6944	0.0533	0.0147
10.0	0.7475	0.0531	0.0197
12.0	0.9070	0.0856	0.0666

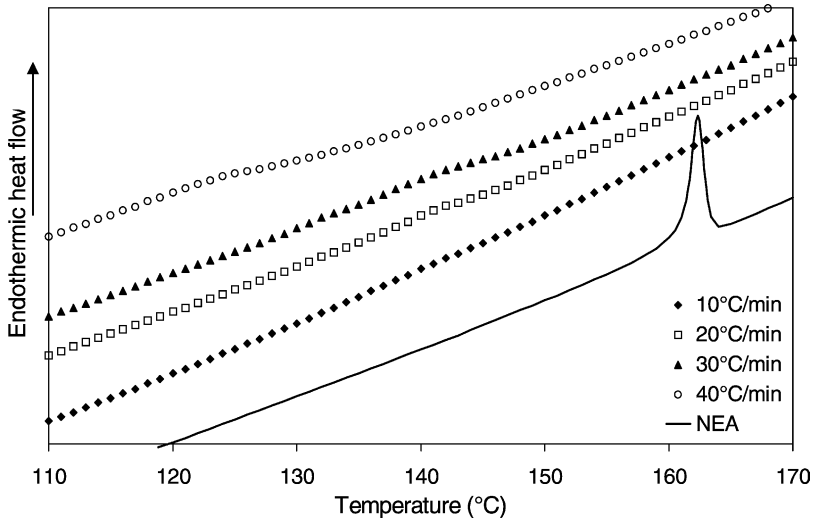

Fig. 10. DSC-curves of 8% NEA containing patches after 2 years crystallised at room temperature and measured at different scanning rates.

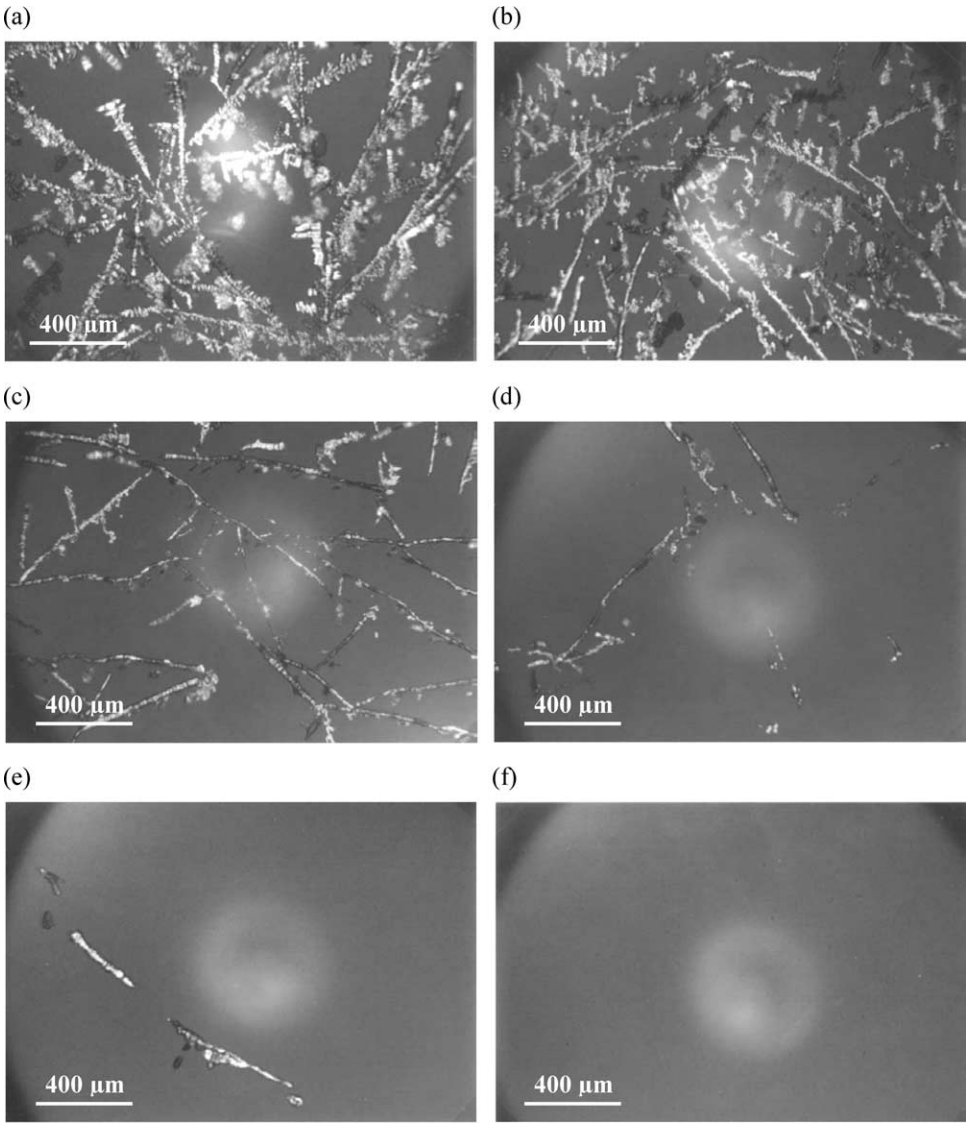

Fig. 11. Polarisation microscopy of 8% NEA containing patches 2 years crystallised at room temperature and heated at different temperatures for 15 min: (a) no heating; (b) 80°C; (c) 100°C; (d) 110°C; (e) 120°C; and (f) 130°C.

the melting peak. Pure NEA exhibited a melting peak at 161°C with a melting heat of 73.2 ± 1.9 J/g (Fig. 10).

An 8% NEA containing patch crystallising at room temperature (Fig. 11a) was investigated by DSC after 2 years using a scanning rate of 10°C/min (Fig. 10). The obtained DSC-curve did not show any melting peak of the recrystallised drug. The placebo system exhibited a phase transition at 89°C, i.e. the matrix softened below the melting point of NEA. Consequently, the crystals slowly dissolved in the polymeric matrix during the heating [10,50], but the sensitivity of DSC was not highly enough to detect the dissolution process of low crystal amounts. The peaks broadened and thus were indistinguishable from the baseline. Especially at low crystal concentrations the melting peak was not detectable or appeared at lower temperatures. We detected DSC-curves typical for solid solutions. The absence of a melting peak often can be considered as an argument for a solid solution.

The drug concentration at which a peak appeared decreased with increasing scanning rate [50]. This is due to the drug having less time to dissolve in the polymer. After an increase in the scanning rate to 40°C/min very small endothermic NEA peaks were detectable in the DSC-curves (Fig. 10). An exact quantitative determination of the amount of crystallised drug content was not possible although an increasing peak area was observable with increasing heating rate. The measured heat was 0.13 J/g matrix for 20°C/min, 0.54 J/g matrix for 30°C/min, and 0.93 J/g matrix for a scanning rate of 40°C/min.

The dissolution of the crystals in the matrix below their melting point was confirmed by simulation by hot stage microscopy. The 8% NEA containing patches were heated for 15 min at different temperatures and observed by polarisation microscopy immediately after heating. The higher the temperature during heating the less crystals were seen (Fig. 11b–f). Already temperatures of 80°C reduced the amount of crystals in the patches because of the higher solubility in the matrix. At 130°C, i.e. below the melting point of NEA, crystals were completely dissolved.

5. Conclusion

Isothermal heat conduction microcalorimetry enables a relatively easy measurement of the crystallisation processes in transdermal patches within a short period of 7 days as well as the determination of the kinetic parameters, such as the rate constant and the mechanism of crystallisation. It was found by this method that the measurable drug-associated heat quantity increases proportionally with an increasing NEA concentration in the concentration range of 4–10% demonstrating a constant crystallisation rate. At a higher supersaturation, such as 12% drug content the crystallisation process is accelerated.

A more specific method to observe the crystal formation is polarisation light microscopy. However, the microscopic analysis requires much longer storage times than microcalorimetry to detect crystallisation.

X-ray powder diffraction so far is the only method for a semi-quantitative determination of the amounts of crystals. On the other hand it is considerably less sensitive than the other two methods.

DSC was not sensitive enough to measure crystallisation state of the examined transdermal patches.

Acknowledgements

The authors want to thank the company Lohmann Therapiesysteme LTS (Andernach, Germany) for the financial support provided and Dr Schnabel, Lohmann Therapiesysteme LTS, for the development and the support to perform the HPLC method.

References

[1] B.C. Finnin, T.M. Morgan, Transdermal penetration enhancers: Applications, limitations, and potential, J. Pharm. Sci. 88 (1999) 955–958.
[2] J. Hadgraft, Passive enhancement strategies in topical and transdermal drug delivery, Int. J. Pharm. 184 (1999) 1–6.
[3] A.F. Davis, J. Hadgraft, Effect of supersaturation on membrane transport: 1. Hydrocortisone acetate, Int. J. Pharm. 76 (1991) 1–8.
[4] M.A. Pellett, A.F. Davis, J. Hadgraft, Effect of supersaturation on membrane transport: 2. Piroxicam, Int. J. Pharm. 111 (1994) 1–6.
[5] N.A. Megrab, A.C. Williams, B.W. Barry, Oestradiol permeation through human skin and silastic membrane: effects of propylene glycol and supersaturation, J. Contr. Rel. 36 (1995) 277–294.
[6] M. Iervolino, S.L. Raghavan, J. Hadgraft, Membrane penetration enhancement of ibuprofen using supersaturation, Int. J. Pharm. 198 (2000) 229–238.
[7] M. Iervolino, B. Cappello, S.L. Raghavan, J. Hadgraft, Penetration enhancement of ibuprofen from supersaturated solutions through human skin, Int. J. Pharm. 212 (2001) 131–141.
[8] F.J.E. Stefano, F.I. Biali, A.F. Scasso, Crystallization in NETA-17β-E2 transdermal patches, Proceed. Int. Symp. Control. Rel. Bioact. Mater. 24 (1997) 703–704.
[9] N.E. Variankaval, K.I. Jacob, S.M. Dinh, Crystallization of β-estradiol in an acrylic transdermal drug delivery system, J. Biomed. Mat. Res. 44 (1999) 397–406.
[10] R. Lipp, A. Müller-Fahrnow, Use of X-ray crystallography for the characterization of single crystals grown in steroid containing transdermal drug delivery systems, Eur. J. Pharm. Biopharm. 47 (1999) 133–138.
[11] J.-H. Kim, H.-K. Choi, Effect of additives on the crystallization and the permeation of ketoprofen from adhesive matrix, Int. J. Pharm. 236 (2002) 81–85.
[12] S. Latsch, T. Selzer, L. Fink, J. Kreuter, Crystallisation of estradiol containing TDDS determined by isothermal microcalorimetry, X-ray diffraction, and optical microscopy, Eur. J. Pharm. Biopharm. SE (2003) 43-52.
[13] P.N. Kotiyan, P.R. Vavia, Eudragits: role as crystallization inhibitors in drug-in-adhesive transdermal systems of estradiol, Eur. J. Pharm. Biopharm. 52 (2001) 173–180.
[14] S.L. Raghavan, A. Trividic, A.F. Davis, J. Hadgraft, Effect of cellulose polymers on supersaturation and in vitro membrane

transport of hydrocortisone acetate, Int. J. Pharm. 193 (2000) 231–237.
[15] X. Ma, J. Taw, C.-M. Chiang, Control of drug crystallization in transdermal matrix system, Int. J. Pharm. 142 (1996) 115–119.
[16] G. Buckton, P. Darcy, Assessment of disorder in crystalline powders – a review of analytical techniques and their application, Int. J. Pharm. 179 (1999) 141–158.
[17] C. Xijun, L. Zhibin, H. Rongzu, Investigation of the crystallization kinetics of cyclotrimethylenetrinitramine and cyclotetramethylenetetranitramine by microcalorimetry, Thermochim. Acta 173 (1990) 193–198.
[18] L.E. Briggner, G. Buckton, K. Bystrom, P. Darcy, The use of isothermal microcalorimetry in the study of changes in crystallinity induced during the processing of powders, Int. J. Pharm. 105 (1994) 125–135.
[19] T. Sebhatu, M. Angberg, C. Ahlneck, Assessment of the degree of disorder in crystalline solids by isothermal microcalorimetry, Int. J. Pharm. 104 (1994) 135–144.
[20] Y. Aso, S. Yoshioka, T. Otsuka, S. Kojima, The physical stability of amorphous nifedipine determined by isothermal microcalorimetry, Chem. Pharm. Bull. 43 (1995) 300–303.
[21] M. Angberg, Lactose and thermal analysis with special emphasis on microcalorimetry, Thermochim. Acta 248 (1995) 161–176.
[22] G. Buckton, P. Darcy, D. Greenleaf, P. Holbrook, The use of isothermal microcalorimetry in the study of changes in crystallinity of spray-dried salbutamol sulphate, Int. J. Pharm. 116 (1995) 113–118.
[23] G. Buckton, P. Darcy, The influence of additives on the recrystallisation of amorphous spray dried lactose, Int. J. Pharm. 121 (1995) 81–87.
[24] M. Pudipeddi, Th.D. Sokoloski, S.P. Duddu, J.T. Carstensen, Calorimetric determination of the heat of precipitation of pseudoephedrine racemic compound – its agreement with the heat of solution, J. Pharm. Sci. 84 (1995) 1236–1239.
[25] H. Ahmed, G. Buckton, D.A. Rawlins, The use of isothermal microcalorimetry in the study of small degrees of amorphous content of a hydrophobic powder, Int. J. Pharm. 130 (1996) 195–201.
[26] H. Ahmed, G. Buckton, D.A. Rawlins, Crystallisation of partially amorphous griseofulvin in water vapour: determination of kinetic parameters using isothermal heat conduction microcalorimetry, Int. J. Pharm. 167 (1998) 139–145.
[27] O.C. Chidavaenzi, G. Buckton, F. Koosha, R. Pathak, The use of thermal techniques to assess the impact of feed concentration on the amorphous content and polymorphic forms present in spray dried lactose, Int. J. Pharm. 159 (1997) 67–74.
[28] V.P. Lehto, E. Laine, A kinetic study on crystallization of an amorphous lubricant, Pharm. Res. 14 (1997) 899–904.
[29] P. Darcy, G. Buckton, Quantitative assessments of powder crystallinity: Estimates of heat and mass transfer to interpret isothermal microcalorimetry data, Thermochim. Acta 316 (1998) 29–36.
[30] P.A. Darcy, J.M. Wiencek, Estimating lysozyme crystallization growth rates and solubility from isothermal microcalorimetry, Acta Cryst. D54 (1998) 1387–1394.
[31] Ch. Gustafsson, H. Lennholm, T. Iversen, Ch. Nyström, Comparison of solid-state NMR and isothermal microcalorimetry in the assessment of the amorphous component of lactose, Int. J. Pharm. 174 (1998) 243–252.
[32] O.C. Chidavaenzi, G. Buckton, F. Koosha, The effect of co-spray drying with polyethylene glycol 4000 on the crystallinity and physical form of lactose, Int. J. Pharm. 216 (2001) 43–49.
[33] K. Kawakami, T. Numa, Y. Ida, Assessment of amorphous content by microcalorimetry, J. Pharm. Sci. 91 (2002) 417–422.
[34] V.-P. Lehto, E. Laine, A kinetik study of polymorphic transition of anhydrous caffeine with microcalorimeter, Thermochim. Acta 317 (1998) 47–58.
[35] M. Avrami, Kinetics of phase change. II Transformation-time relations for random distribution of nuclei, J. Chem. Phys. 8 (1940) 212–224.
[36] B. Hutchinson, S. Jonsson, L. Ryde, On the kinetics of recrystallisation in cold worked metals, Scr. Met. 23 (1989) 671–676.
[37] A. Maffezzoli, J.M. Kenny, L. Torre, On the physical dimensions of the Avrami constant, Thermochim. Acta 269/270 (1995) 185–190.
[38] M.C. Weinberg, D.P. Birnie III, Avrami exponents for transformations producing anisotropic particles, J. Non-Cryst. Solids 202 (1996) 290–296.
[39] R.V. Muraleedharan, Variation of slope in Avrami plots, Scripta Mater. 40 (1999) 1367–1370.
[40] M.R. Mazzobre, G. Soto, J.M. Aguilera, M.P. Buera, Crystallization kinetics of lactose in systems co-lyofilized with trehalose. Analysis by differential scanning calorimetry, Food Res. Int. 34 (2001) 903–911.
[41] J. Vázquez, P.L. López-Alemany, P. Villares, R. Jiménez-Garay, Generalization of the Avrami equation for the analysis of non-isothermal transformation kinetics. Application to the crystallization of the $Cu_{0.20}As_{0.30}Se_{0.50}$ alloy, J. Phys. Chem. Solids 61 (2000) 493–500.
[42] F. Ye, K. Lu, Crystallization kinetics of Al-Na-Ni amorphous alloy, J. Non-Cryst. Solids 262 (2000) 228–235.
[43] T. Pradell, C. Crespo, N. Clavaguera, M.T. Clavaguera-Mora, Diffusion controlled grain growth in primary crystallization: Avrami exponents revisited, J. Phys. Condens. Matter 10 (1998) 3833–3844.
[44] M. Avrami, Kinetics of phase change. I General theory, J. Chem. Phys. 7 (1939) 1103–1112.
[45] M. Angberg, Ch. Nyström, Evaluation of heat-conduction microcalorimetry in pharmaceutical stability studies. I. Precision and accuracy for static experiments in glass vials, Acta Pharm. Suec. 25 (1988) 307–320.
[46] L.D. Hansen, E.A. Lewis, D.J. Eatough, R.G. Bergstrom, D. De-Graft-Johnson, Kinetics of drug decomposition by heat conduction calorimetry, Pharm. Res. 6 (1989) 20–27.
[47] M.J. Koenigbauer, Pharmaceutical applications of microcalorimetry, Pharm. Res. 11 (1994) 777–783.
[48] R.J. Willson, A.E. Beezer, J.C. Mitchell, W. Loh, Determination of thermodynamic and kinetic parameters from isothermal heat conduction microcalorimetry: applications to long-term-reaction studies, J. Phys. Chem. 99 (1995) 7108–7113.
[49] T. Selzer, M. Radau, J. Kreuter, Use of isothermal heat conduction microcalorimetry to evaluate stability and excipient compatibility of a solid drug, Int. J. Pharm. 171 (1998) 227–241.
[50] G.R. Lloyd, D.Q.M. Craig, A. Smith, An investigation into the melting behavior of binary mixes and solid dispersions of paracetamol and PEG 4000, J. Pharm. Sci. 86 (1997) 991–996.